ISSN 1 746-7233, England, UK
World Journal of Modelling and Simulation
Vol. 14 (2018) No. 2, pp. 108-123

Computational fluid dynamical analysis of turbulent heat transfer in a channel fitted with staggered V-Shaped baffles*

Younes Menni[1†], Ahmed Azzi[1]

[1]Unit of Research on Materials and Renewable Energies, Department of Physics, Faculty of Sciences, Abou Bekr Belkaid University, BP 119-13000-Tlemcen, Algeria

(*Received July 18 2016, Accepted December 21 2017*)

Abstract. This is an original work as it uses a novel method for improving the heat transfer in a completely new flow geometry. The present research aims to conduct a computational fluid dynamical analysis on a turbulent-flow forced convection, in the presence of two transverse 45^0 V-upstream baffles, placed in an overlapping manner, inside a horizontal two-dimensional rectangular section channel. The channel width to height aspect ratio, channel length-to-aeraulic diameter, V-baffle spacing-to-channel height ratio, and V-baffle height to channel height blockage ratio are fixed at $W/H = 1.321$, $L/D_h = 3.317$, $P_i/H = 0.972$, and $h/H = 0.547$, respectively. The Reynolds number is varied from 12,000 to 32,000. The mathematical equations that describe the fluid flow and heat transfer in the computational domain, i.e., continuity, momentum, and energy, were solved using the finite volume method with the standard k- model to describe the turbulence. Thermo-aerodynamic fields, axial velocity profiles, skin friction coefficients, local and average Nusselt numbers, and thermal enhancement factors were obtained, investigated and analyzed numerically. By comparing with those implemented in practice, our numerical results are very agreeable. This simulation can be applied in improving the thermal efficiency of heat exchangers as well as solar air baffled channel collectors.

Keywords: fluid mechanics, heat transfer, governing equations, numerical simulation, baffles and fins

1 Introduction

Baffles and fins at low, moderate, and high flow Reynolds number values play a major role in the industry these days. Several analyses and investigations, by means of numerical and experimental techniques, were conducted, in this topic, in order to enhance their position, their length, their height, their thickness, their attack angle, their inclination, their orientation, and their form. A numerical investigation was carried out by Kelkar and Ptankar[12], for a constant property fluid having a laminar flow through a parallel-plate duct with staggered fins. Computations were performed for different values of the Reynolds number, the Prandtl number, geometric parameters, and the fin-conductance parameter. Habib et al.[14] made experiments to study the characteristics of the turbulent flow and heat transfer within the periodic cell existing between the segmental baffles staggered within a rectangular channel. The influence of the baffle size and Reynolds number on the coefficients of the local heat transfer and global heat transfer, along with the pressure drop measurements was described. Berner et al.[7] used the Laser Doppler Anemometry (LDA) technique to get some experimental values of the average velocity and turbulence distributions in the turbulent regime throughout a duct with many segmented baffle plates. The authors aimed at determining the number of baffles that are needed to have the periodic boundary condition and to determine the relationship between the flow rate and the geometry. Experimental results of velocity and wall pressure fluctuations in the turbulent flow through a simulated tube bank with square arrangement, after

* This research was funded by the Research Unit of Materials and Renewable Energies, Abou Bekr Belkaid University, Republic of Algeria. The authors would like to thank Assoc. Prof. Dr. Ahmed AZZI suggestions

† Corresponding author. *E-mail address*: menniyoues.cfd@gmail.com.

passing a baffle plate were performed by M?ller et al.[30], using hot wires and a pressure transducer. Behavior of fluctuating quantities was described by means of dimensionless autospectral density functions and their interdependence was discussed. A numerical and experimental study was carried out by Demartini et al.[13] on air flow inside a channel with a rectangular cross section with two baffle plates mounted on the upper and lower walls. This study included also a comprehensive investigation of the velocity and pressure profiles. The solution to the problem was found by the Hot Wire Anemometry technique and the Finite Volume method using the commercial program FLUENT 5.2. Lopez et al.[10] reported the numerical investigation of laminar forced convection heat transfer in a three-dimensional channel with baffles, using the periodically fully developed flow conditions of Patankar[31]. The authors pointed out that the three-dimensional effects on the friction factor of a channel, which has a unity aspect ratio and a blockage ratio equal to 0.5, increased as the Reynolds number went up. The three-dimensional laminar forced-convection flow was investigated by Guo and Anand[46] in a duct having one single baffle in the intake region. The impact of the Reynolds number, Prandtl number, baffle height and thermal conductivity ratio were examined. In general, both separation and recirculation lengths around baffles increase with an increase in the flow Reynolds number and baffle height. In addition, the spanwise averaged Nusselt number increased with an increase in the thermal conductivity of the wall. The fluid flow and heat transfer through staggered wall-mounted two-dimensional obstacles, put on the bottom and top walls of the channel, were attentively examined by Mohammadi Pirouz et al.[15], using the Lattice Boltzmann Method (LBM). The authors concluded that the Lattice Boltzmann Method (LBM) is well suited for studying the heat transfer in conjugate problems. Tsay et al.[35] numerically investigated the heat transfer enhancement due to a vertical baffle in a backward-facing step flow channel. They analyzed the effects of the geometrical parameters of the model as well as the functioning parameters on the structure of flow. The authors demonstrated that the mean value of Nusselt number could be increased by 190% by installing a baffle into the field. The numerical results obtained also proved that the flow considerations and the heat transfer characteristics are highly dependent on the location of the baffle inside the channel. Nasiruddin and Kamran Siddiqui [17] indicated that the convective heat transfer in a heat exchanger tube may be enhanced by placing a baffle inside the tube. The investigators considered a comparative study between three different baffle orientations. The first case examined a vertical baffle. The second case investigated a baffle inclined towards the upstream end, and the third one considered a baffle inclined towards the downstream end. The results suggested that a baffle inclined towards the downstream side with a smaller inclination angle (15° in their study) is a better choice as it enhances the heat transfer by a similar magnitude with a minimal pressure loss. An experimental investigation of frictional loss and heat transfer behavior of turbulent flow in a rectangular channel with a single inclined perforated baffle and with an isoflux heating from the upper surface was presented by Dutta and Dutta[20]. In that study, the effects of inclined baffle perforation density, size, position, and orientation were studied for internal cooling heat transfer augmentation. In another experiment, Karwa and Maheshwari[24] investigated fully (open area ratio of 46.8%) and half (open area ratio of 26%) perforated baffles covering Re values ranging from 2,700 to 11,150. The study showed an enhancement of 79-169% in Nusselt number over the smooth duct for the fully perforated baffles and 133-274% for the half perforated baffles while the friction factor for the fully perforated baffles are 2.98-8.02 times of that for the smooth duct and is 4.42-17.5 times for the half perforated baffles. In general, the half perforated baffles are thermo-hydraulically better to the fully perforated baffles at the same pitch. Of all the configurations studied, the half perforated baffles at a relative roughness pitch of 7.2 give the greatest performance advantage of 51.6-75% over a smooth duct at equal pumping power. Ary et al.[5] used the CFX 10 commercial software to analyze numerically the heat transfer and associated frictional head loss in a rectangular channel with 5° inclined diamond hole type perforated baffles. Experimental investigations were also carried out to confirm the predicted characteristics of heat transfer enhancement and associated frictional head loss for a single baffle and two baffles, respectively. Other similar works can be found in the literature as Motlagh and Moghimi[19], Saini and Pratibha[2], Kumar et al.[27], Das and Chakrabarti[32], Naveed Ahmed1 et al[16], Saini et al.[1], and Elangovan and Selvaraj[11].

A detailed examination of the impact of the obstacle geometry reconfiguration, has been conducted by other authors, on the fluid flow and heat transfer characteristics in some particular cases of air flow geometry, for example simple flat rectangular[43, 45], corrugated[44], rounded[42], graded [26], $'L'$[36], waisted triangular[40],

arc[39], diamond[38], cascaded[37, 41], $'V'$[33], double $'V'$[34], and $'Z'$[29] shaped. Different geometry parameters and various operating conditions were used in the previous studies.

The topic is of paramount importance. Heat exchangers are used in several sectors and in very diverse fields. The improvement of their performance has been and is still of major concern to theorists and practitioners. The issue of exchanging heat between two fluids within a heat exchanger relies mainly on the value of the heat transfer coefficient. This coefficient is a mine of factors that affect the heat exchange between two media. Therefore, it is an ambitious attempt to work on such a topic. The main objective of the current computational fluid dynamical simulation is to analyze numerically the dynamic and thermal behavior of a constant property Newtonian fluid (air) via placement of two heated upper and insulated lower wall-mounted, staggered, transverse, V-upstream shaped, solid-type baffles. The finite volume approach proposed by Patankar[21], with the k-epsilon model developed by Launder and Spalding[4], by means of Commercial CFD software FLUENT, is applied in this contribution. Thermal and aerodynamic fields, axial profiles of velocity, heat transfer coefficients, skin friction coefficients, and thermal enhancement performance evaluations are investigated and analyzed for the stations selected along the whole domain investigated, namely, upstream, downstream and between the two V-baffles.

2 Mathematical formulation

2.1 Problem definition

This contribution is performed in a 2D field, which represents a horizontal rectangular cross section channel of $L = 0.554m$ length, $H = 0.146m$ height, and $D_h = 0.176m$ aeraulic diameter, where two heated upper and insulated lower wall-attached, staggered, transverse, V-shaped, solid-type baffles were inserted into the channel. A geometric view of the present baffled channel is shown in Fig. 1a with Cartesian coordinates.

The flow is 2D, turbulent, incompressible, Newtonian and in steady state with no radiation heat transfer, and neglecting viscous dissipation. The thermo-physical properties of the fluid (ρ, C_p, μ, and λ_f) are constant. The Prandtl number is taken equal to 0.71. The standard $k-\varepsilon$ turbulence model of Launder and Spalding[4] is adopted to simulate the turbulent forced-convection fluid flow comportment by using the Commercial CFD software FLUENT.

To enhance the heat transfer in the computational domain, two V-upstream shaped baffles with an angle of attack of value of $\alpha = 45^\circ$ are mounted in a staggered manner on the insulated lower and heated upper surfaces of the channel. The first V-baffle was placed on the heated top wall of the channel at the distance of $L_1 = 0.218m$ downstream of the inlet while the second V-baffle inserted to the insulated bottom wall at $L_2 = 0.174m$ upstream of the channel outlet. The distance between the top edge of the V-baffle and the channel surface was kept constant at $h = 0.08m$. The axial pith, P_i or separation distance between the baffles is set to 0.142m. The thickness of etch V-baffle is $w = 0.01m$. The structural dimension of the present baffled channel, cited above, is the same described in Demartini et al.[13] used for validation. The detailed of the boundary conditions are also shown in Fig. 1 (see Fig. 1b). Air is the working fluid, flows through the channel with a uniform inlet-velocity profile and a constant temperature, atmospheric pressure with zero pressure gradients at the channel outlet and no slip wall boundary conditions are taken for the current contribution.

A non-uniform mesh, with quadrilateral-type, structured cells in the two-directions is used. Fig. 1c presents a mesh used near the solid channel surfaces, in the presence of the flow deflectors. The mesh is too fine near the all solid boundaries[13]. This refinement was necessary to resolve the strong velocity and temperature gradients in that region[13]. For the regions more distant from the walls, the mesh is uniform[13]. To examine the impact of the mesh density on the resolution of the numerical method used, different cell numbers are investigated and a cell of 245 (in X-direction) 95 (in Y-direction) is selected for the rest of our study.

2.2 Governing equations

The turbulent forced-convection heat transfer phenomenon under consideration is governed by the steady 2D shape of continuity, momentum, and energy equations. In the Cartesian tensor system these equations can be written as follows[21]:

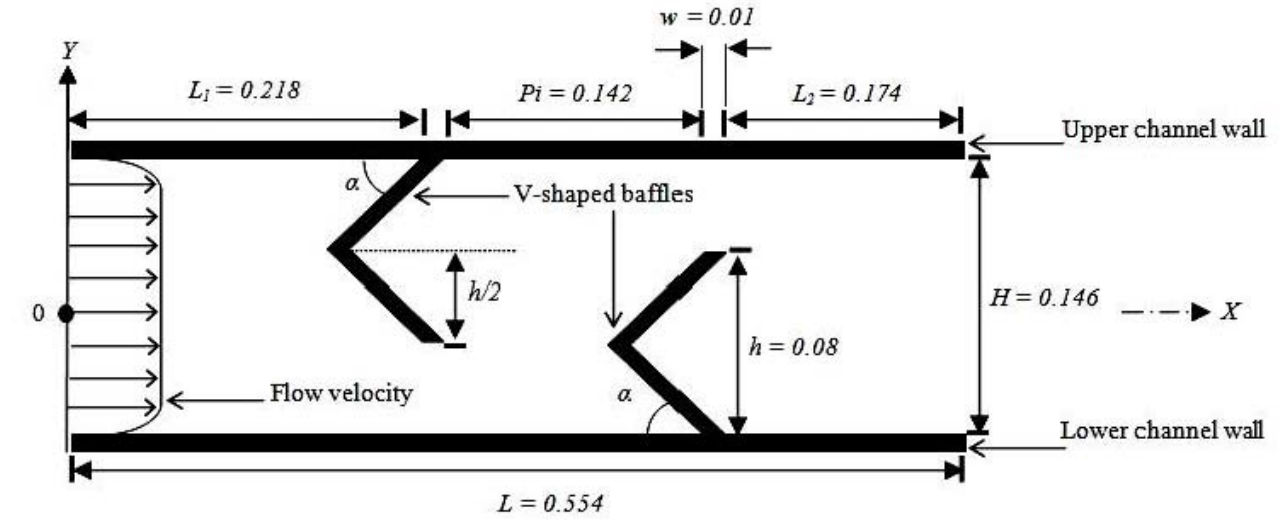

(a)

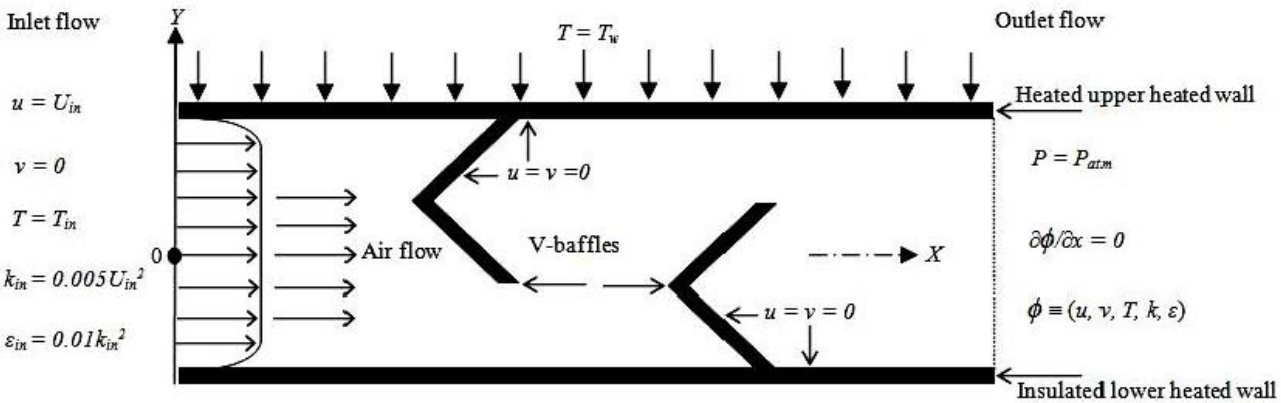

(b)

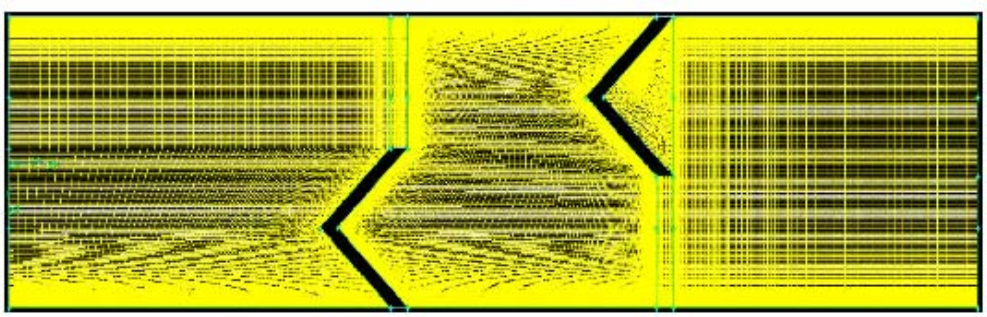

(c)

Fig. 1: (a) Present baffled channel (dimension in m), (b) boundary conditions, and (c) mesh structure

Continuity equation:

$$\frac{\partial u_j}{\partial x_j} = 0. \tag{1}$$

Continuity equation:

$$\rho u_j \frac{\partial u_i}{\partial x_j} = -\frac{\partial P}{\partial x_i} + \frac{\partial}{\partial x_j}\left(\mu \frac{\partial u_i}{\partial x_j} - \rho \overline{u_i' u_j'}\right) \tag{2}$$

where ρ is the fluid density, P is the pressure, μ is the dynamic viscosity, u_i and u_j are mean velocity components in xi and x_j directions, u_i' and u_j' are fluctuation velocity components in x_i and x_j directions.

Where

$$-\rho\overline{u_i'u_j'} = \mu_t\left(\frac{\partial u_i}{\partial x_j}+\frac{\partial u_j}{\partial x_i}\right)-\frac{2}{3}\rho\delta_{ij}k. \tag{3}$$

Energy equation:

$$\rho u_j\frac{\partial T}{\partial x_j} = \frac{\partial}{\partial x_j}\left((\Gamma+\Gamma_t)\frac{\partial T}{\partial x_j}\right) \tag{4}$$

where Γ and Γ_t are molecular thermal diffusivity and turbulent thermal diffusivity, respectively and are given by

$$\Gamma = \frac{\mu}{\mathrm{Pr}} \quad \text{and} \quad \Gamma_t = \frac{\mu_t}{\mathrm{Pr}_t} \tag{5}$$

where μ_t is the turbulent viscosity, defined as

$$\mu_t = \rho C_\mu\frac{k^2}{\varepsilon}. \tag{6}$$

δ_{ij} the Kroenecker delta, and k the kinetic energy of the turbulence, defined as

$$k = \frac{1}{2}\overline{u_i'u_i'} \tag{7}$$

where C is an empirical constant. The steady state transport equations of the standard $k-\varepsilon$ model are expressed as

Turbulent kinetic energy k:

$$\rho u_j\frac{\partial k}{\partial x_j} = \frac{\partial}{\partial x_j}\left[\left(\mu+\frac{\mu_t}{\sigma_k}\right)\frac{\partial k}{\partial x_j}\right]+G_k-\rho\varepsilon. \tag{8}$$

Dissipation rate ε:

$$\rho u_j\frac{\partial \varepsilon}{\partial x_j} = \frac{\partial}{\partial x_j}\left[\left(\mu+\frac{\mu_t}{\sigma_\varepsilon}\right)\frac{\partial \varepsilon}{\partial x_j}\right]+C_{1\varepsilon}\frac{\varepsilon}{k}G_k-C_{2\varepsilon}\rho\frac{\varepsilon^2}{k} \tag{9}$$

where

$$C_\mu = 0.09, C_{1\varepsilon} = 1.44, C_{2\varepsilon} = 1.92, \sigma_k = 1.0, and \sigma_\varepsilon = 1.3 \tag{10}$$

are the constants of the turbulence model[4], and G_k is the production rate of the kinetic energy due to the energy transfer from the mean flow to turbulence.

2.3 Boundary conditions

A uniform one-dimensional profile of velocity is introduced at the inlet region of whole domain investigated[13, 17] while an atmospheric pressure-outlet condition is applied at the exit[13], as shown in Fig. 1b. The turbulence intensity was kept at 2% at the inlet[13]. The pressure at the inlet of the computational domain was set equal to the zero (gauge)[17]. No-slip and impermeability boundary conditions were applied over the heated upper and insulated lower channel walls as well as the 45° V-shaped baffle surfaces[13]. A constant temperature of 102°C ($T_w = 375K$) was applied on the upper surface of the channel as the thermal boundary conditions[17]. The lower channel wall is adiabatic. The temperature of air was set equal to 27°C ($T_{in} = 300K$) at the inlet of the channel[17]. All boundary conditions are presented as

At the inlet ($x = 0$),

$$u = U_{in}, v = 0 \tag{11}$$

$$k_{in} = 0.005U_{in}^2 \tag{12}$$

$$\varepsilon_{in} = 0.1k_{in}^2 \tag{13}$$

$$T = T_{in} \tag{14}$$

where k_{in} stands for the entrance condition for turbulent kinetic energy, and ε_{in} is the inlet condition for turbulent energy dissipation rate.

In the channel outlet ($x = L$) it is prescribed the atmospheric pressure, P_{atm} with zero-gradient conditions.

$$P = P_{atm} \tag{15}$$

$$\frac{\partial \phi}{\partial x} = 0 \tag{16}$$

in which ϕ is a variable used to represent quantities such as velocity components u and v, temperature T, turbulent kinetic energy k or turbulent energy dissipation rate ε.

For the channel walls it is imposed

$$u = v = 0 \tag{17}$$

$$k = \varepsilon = 0 \tag{18}$$

$$T = T_{in} \quad \text{for the upper channel wall} \tag{19}$$

$$\frac{\partial T}{\partial Y} = 0 \quad \text{for the lower channel wall} \tag{20}$$

At the fluid-wall points of the all computational domain, the following conditions are applied:

$$\lambda_f \frac{\partial T_f}{\partial n} = \lambda_s \frac{\partial T_s}{\partial n} \tag{21}$$

$$T_f = T_S \tag{22}$$

where λ_f and λ_s are thermal conductivities of fluid and solid, respectively.

The Reynolds number, Re calculated with the aeraulic diameter[8]

$$D_h = 4HW/2(H + W) \tag{23}$$

and the entrance velocity $\overline{U}$ is taken according to the experiments of Demartini et al.[13]. It is equal to 8.7310^4. This dimensionless parameter is defined as follows[13]:

$$\mathrm{Re} = \frac{\rho \overline{U} D_k}{\mu} \tag{24}$$

The skin friction coefficient, Cf can be obtained by[28]

$$Cf = \frac{\tau_w}{\frac{1}{2}\rho \overline{U}^2} \tag{25}$$

The friction factor, f is evaluated from the pressure drop, $\triangle P$ across the length of the channel, L as[28]

$$f = \frac{(\Delta P/L) D_h}{\frac{1}{2}\rho \overline{U}^2} \tag{26}$$

The local Nusselt number Nu_x is given by[26]

$$Nu_x = \frac{h_x D_h}{\lambda_f} \tag{27}$$

The average Nusselt number, $\overline{Nu}$ is computed with the following equation[26]:

$$\overline{Nu} = \frac{1}{L}\int Nu_x \partial x \tag{28}$$

where h_x is the local convective heat transfer coefficient.

3 Numerical solution

The governing equations with the associated boundary conditions were solved using the Finite Volume Method (FVM), details of which can be found in Patankar[21], in two-dimensions, employing the Commercial CFD software FLUENT, with the standard $k-\varepsilon$ model of Launder and Spalding[4] to describe the turbulence phenomenon. The method uses staggered grids and artesian velocity components, handles the pressure-velocity coupling with the SIMPLE-algorithm and solves the resulting system of equations iteratively with a Tri-Diagonal-Matrix Algorithm (TDMA), as indicated by Valencia and Cid[3]. Considering the characteristics of the flow, the QUICK scheme, proposed by Leonard and Mokhtari[6], was applied to the interpolations, while a Second-Order Upwind-scheme[21] was used for the pressure terms, as indicated in[13]. A non-uniform, quadrilateral-type grid in the two-directions was inserted. To control the update of the computed variables at etch iteration, under-relaxation was varied between 0.3 and 1.0[17]. The under-relaxation factor was carefully chosen to prevent large variations in the source terms. The solution was assumed to be converged when the following criterion was satisfied as[25]

$$Max\left(\frac{|\phi-\phi^*|}{|\phi^*|}\right) \leq \delta \tag{29}$$

where $*$ denote the previews iteration value, and δ is a prescribed error. For the present simulation, we select $\delta = 10^{-9}$ for $\phi(u, v, k, \varepsilon)$ and $\delta = 10^{-12}$ for $\phi(T)$.

3.1 Mesh verification

The grid independence tests were performed by realizing CFD simulations in the whole domain investigated, using different structured quadrilateral-type grid systems with the number of mesh nodes ranging from 35 to 145 along the pipe depth and 95 to 370 along the length. In particular, the numerical values of average Nusselt number (Nu), and skin friction factor (f) are shown plotted in Fig. 3 (a), and (b) versus the mesh node density (95 35; 120 45; 145 55; 170 65; 195 75; 220 85; 245 95; and 370 145), for $Re = 8.7310^4$, respectively. The grid system with the number of nodes equal to 245 95 (in X and Y directions respectively) performs around 0.350 %, and 0.392 % deviation for the Nu, and f, respectively, in compared with the grid of size 370 145. Therefore, the grid cell of 245 95 is selected for the rest of our study.

3.2 Numerical validation

The results obtained from our computational fluid dynamical analysis using the FLUENT are validated through comparison with the numerical and experimental results reported by Demartini et al.[13] which are available in the literature. For this reason, the same conditions are kept. Fig. 2a gives the validation plot of the axial velocity (U) for $Re = 8.7310^4$, respectively. Both the numerical and experimental profiles of U are

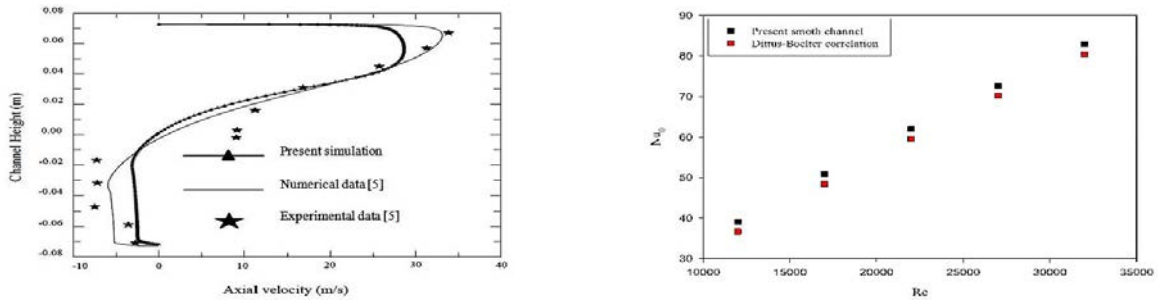

(a) (b)

Fig. 2: Validation of (a) axial velocity profiles at $x = 0.525$ m, and (b) smooth channel average Nusselt number at the heated upper channel wall, with reported data.

measured along the channel depth at the locations $x = 0.525$ m from entrance, respectively. As observed on these figures, our numerical results are very agreeable.

The current computational fluid dynamical analysis results on heat transfer are also validated by comparing the predicted Nusselt number (Nu_0) with the results obtained from the well-known steady-state flow correlation of Dittus-Boelter[9] for the turbulent forced-convection smooth channel flow. The Nu_0 obtained from the present smooth channel and the correlation of Eq. (30) at Reynolds numbers of $1.2 10^4 - 3.2 10^4$ are plotted in Fig. 2b.

$$Nu_0 = 0.023 Re^{0.8} Pr^{0.4} \quad for \;\; Re \geqslant 10^4. \tag{30}$$

As it can be shown in this figure, the present smooth channel results agree well with the available correlation with 3.5 % in comparison with Dittus-Boelter correlation for the Nu_0.

4 Results and discussion

4.1 Fluid flow

The flow pattern of air in the rectangular channel with staggered V-upstream shaped baffles on the heated upper and insulated lower walls can be shown by considering the streamlines and axial velocity fields as presented, respectively, in Fig. 3 at five different values of Reynolds number (12,000, 17,000, 22,000, 27,000, and 32,000). It is shown in Fig. 3 that the thermo-aeraulic fields are the most notable behavior of the impacts of the 45° V-upstream shaped baffles on the main flow direction, i.e., flow separation, recirculation, and reattachment. The comparison of velocity values at different flow rates in terms of Reynolds numbers shows that as the air is redirected near the heated upper and insulated lower wall-mounted 45° V-upstream shaped baffles, a strong recirculation zone is formed behind of the heated upper wall-attached V-baffle, which was induced due to the flow separation[17]. The recirculation was located close to the solid wall and its height was approximately equal to the extent of the flow blockage[17] by the considered baffle, which is equal to 0.08m for our study. A similar phenomenon is observed near the second V-baffle with recirculation cells at the corner behind the insulated lower wall-placed V-baffle, responsible for the high flow velocities observed at the outlet of the computational domain, creating a negative velocity profile which introduces mass inside the test channel through the outlet[13]. As expected, there is a direct correlation between the increase in the Reynolds number and the elevation in the fluid flow velocity.

Fig. 4 shows the axial profiles of velocity in transverse sections at positions $x = 0.159m$ and $x = 0.189m$ from entrance for $= 45^\circ$ and $Re = 12,000$. These sections are situated upstream of the top wall V-baffle (first V-baffle), located at $x = 0.218m$, measured downstream of the entrance. In the figure, it is visible that the deformation of the airflow field increases as the flow approaches the top wall V-baffle. In the zone between

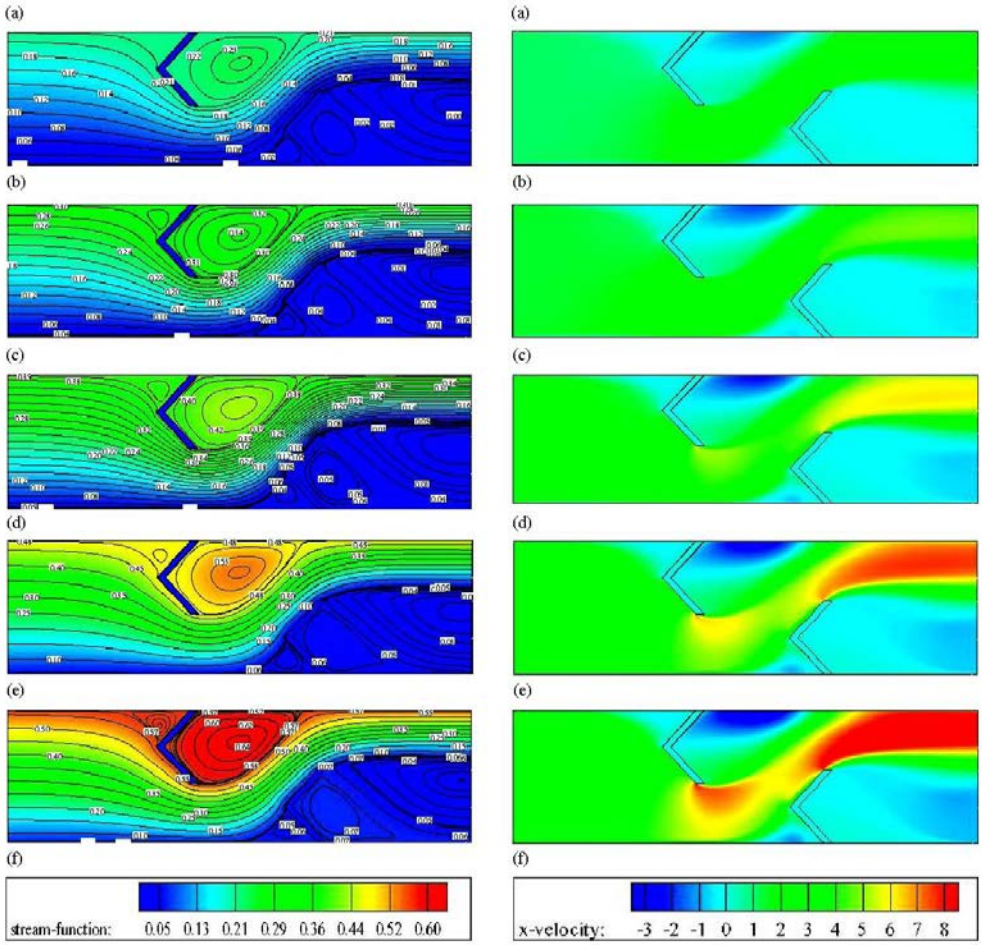

Fig. 3: Variation of streamlines and axial velocity fields with Reynolds number.

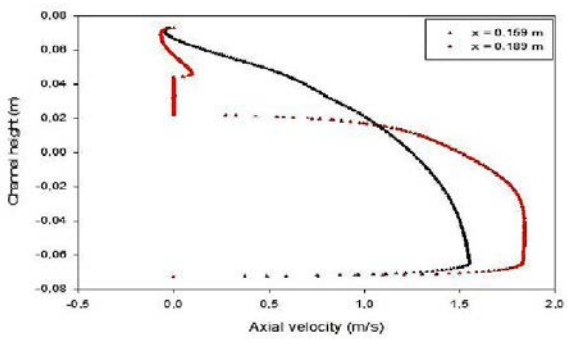

Fig. 4: Axial velocity profiles upstream of the first 45° V-shaped baffle for $Re = 12,000$

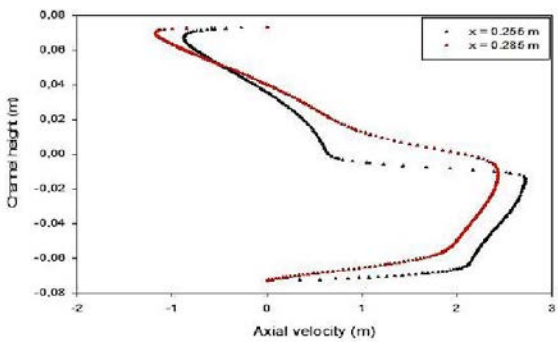

Fig. 5: Axial velocity profiles between the two 45° V-shaped baffles for $Re = 12,000$

the tip of the considered baffle and the bottom channel wall, the velocity is increased. This is confirmed by Demartini et al.[13].

In the region downstream of the heated top wall-mounted $45°$ V-upstream baffle, at stations given by $x = 0.255m$ and $x = 0.285m$ from entrance, a recirculation cell with very low velocity values (negative velocities) are observed[13], as shown in Fig. 5. Its velocity is reduced in the upper half of the channel, while in the lower part is increased[13], reaching $2.72m/s$, 2.591 times higher than the entrance velocity, which is $1.04963m/s$ at $Re = 12,000$.

The axial velocity profiles of the airflow at distances equal to 0.055m and 0.025m before the insulated bottom wall-mounted $45°$ V-upstream baffle (second baffle), corresponding to positions $x = 0.315m$ and

$x = 0.345m$, measured downstream of the entrance, and according to the Fig. 6, the numerical results show that for a constant value of the Reynolds number ($Re = 12,000$), as the airflow is redirected near the insulated bottom wall-attached V-baffle, a very small recirculation cell is formed in the vicinity of the lower left corner, while in the upper part the flow starts to accelerate toward the gap above the second V-baffle, in accordance with the results by Demartini et al.[13].

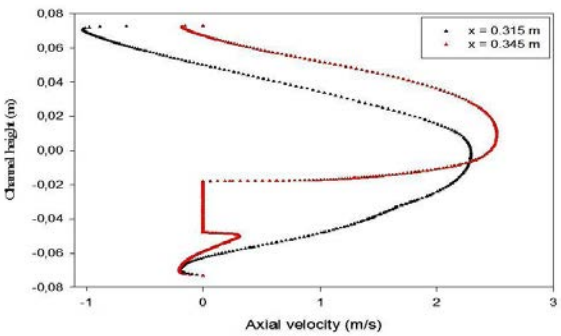

Fig. 6: Axial velocity profiles upstream of the second 45° 45° V- baffle for $Re = 12,000$

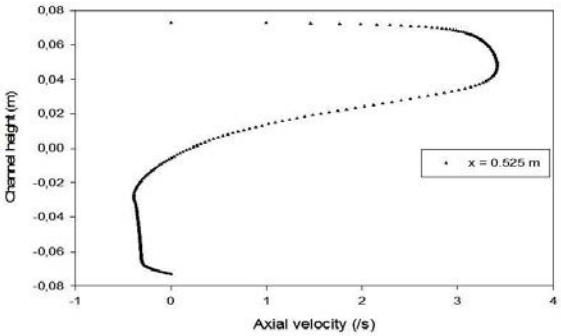

Fig. 7: Axial velocity profiles after the second 45° V-shaped, near the outlet for $Re = 12,000$

Fig. 7 shows the computational results of axial velocity distributions after the insulated bottom wall-placed 45° V-upstream baffle, near the channel outlet when $Re = 12,000$. At a station $x = 0.525m$, $0.029m$ before the exit, the airflow is characterized by very high velocities behind the second V-baffle in the upper part of the channel, near the top wall with an acceleration process that starts after the second baffle[13], approaching 327% of the inlet velocity. These values are only possible due[13] to very strong flow recirculation on the back side of the insulated bottom wall-mounted 45° V-shaped baffle, which leads air from outside of the channel into the test section.

Numerical results of axial velocity profiles versus the Reynolds number for positions $x = 0.159m, 0.189m, 0.255m, 0.285m, 0.315m$, and $0.525m$, measured downstream of the entrance in the plain channel with two 45° staggered V-upstream baffle, are shown in Fig. 8(a)-(f), respectively. The flow was simulated for the Reynolds numbers of 12,000, 17,000, 22,000, 27,000, and 32,000. As expected, obviously it can be observed that values of axial velocity become higher with increasing values in Reynolds number. In the figures, the comparison of axial velocity at various Reynolds numbers from 12,000 to 32,000 shows that as the airflow approaches the first V-deflector, its velocity is reduced in the upper part of the channel while in the lower part is increased. Negative values observed in the numerical results from the location $x = 0.189m$ indicate the presence of a small vortex at the corner in front of the heated top wall-mounted V-upstream baffle, as shown in Fig. 8a and 8b. In the intermediate zone, as a result of sudden expansion in the cross-section, the air separates, a larger recirculation is observed behind the considered V-upstream baffle in the top half of the channel and the flow reattachment is then established, as indicated in Fig. 88c and 8d. This behavior is confirmed in[15]. The patterns take the same form near the second V-deflector mounted on the insulated bottom channel surface and illustrate the increased concentration of recirculation cells in the lower half of the channel at the highest value of Reynolds number ($Re = 12,000$), a small one in the vicinity of the lower left corner (see Fig. 8e) while the most intense is that occurring behind the insulated bottom surface-mounted 45°V-upstream baffle (see Fig. 8f). The recirculation cells behind the V-baffles cause the air fluid to strongly rotating motion, as indicated and confirmed in[28]. This motion causes the fluid near the wall to flow in the core region and vice versa[28]. These recirculation cells increase in its size and occupy more and more the space near to the baffles[18]. This result can be explained by the fact of the velocity increases of air flow and also the convective heat transfer from the surface of the channel wall to the following air[25].

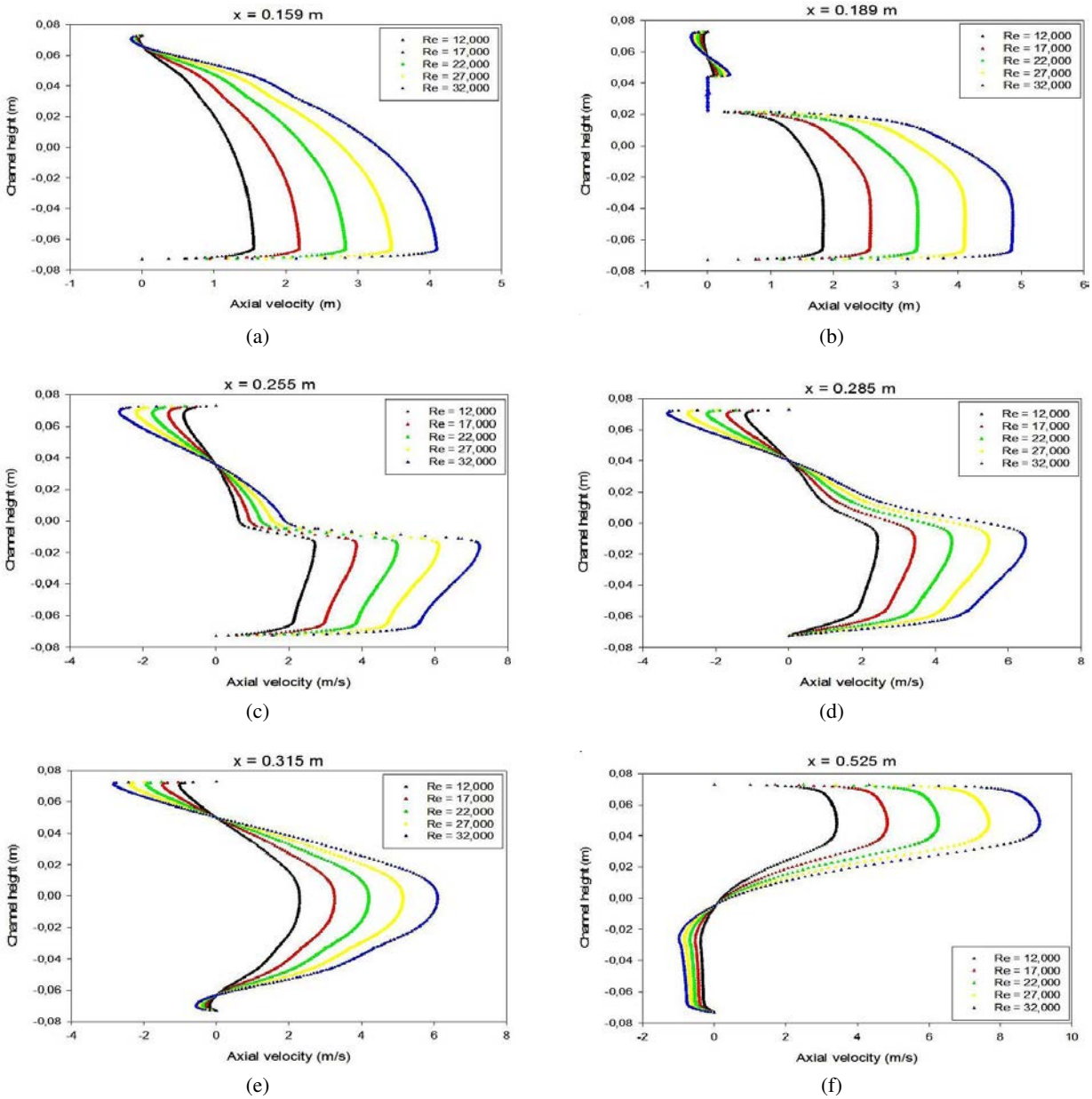

Fig. 8: Axial velocity profiles versus Reynolds number for different axial stations, (a) $x = 0.159m$, (b) $x = 0.189m$, (c) $x = 0.255m$, (d) $x = 0.285m$, (e) $x = 0.315m$, and (f) $x = 0.525m$.

4.2 Heat transfer

The presence of the $45°$ V-upstream baffles influences not only the velocity field but also the temperature distribution in the computational domain examined. The contour plots of temperature field in the air baffled channel for the same range of Reynolds numbers ($Re = 12,000, 17,000, 22,000, 27,000$, and $32,000$) are shown in Fig. 9(a)-(e), respectively.

Numerical results show very high temperature values adjacent to the V-deflectors. In the vortex regions, the fluid temperature is significantly high as compared to that in the same region of no baffle case[17]. This means that the vortex flows provide a significant influence on the temperature field, because they can induce better fluid mixing between the wall and the core regions, leading to a high temperature gradient along over the heating wall[28]. In the regions between the tip of the V-baffles and the channel walls, the temperature is decreased. Due to the changes in the airflow direction produced by the V-baffles, the highest temperature values appear near the heated upper wall-mounted V- baffle corners, where the vortices occur with an acceleration process that starts

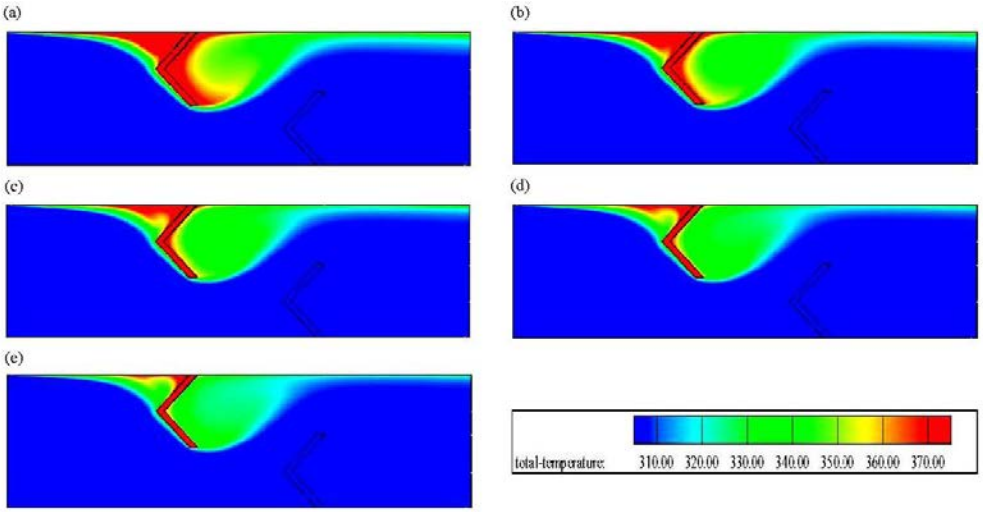

Fig. 9: Variation of streamlines and axial velocity fields with Reynolds number.

just after the second V-deflector. Concerning the effect of the flow rate in terms of Reynolds numbers on the temperature field, it can see from this figure and for this attack angle ($= 45°$), that when the Reynolds numbers increases from 12,000 to 32,000, the temperature contours become thoroughly denser, which yields to the removal of higher quantities of energy from deflector faces[15]. As expected, the V-baffles surface temperature decreases, while Reynolds number rises. It is concluded that the presence of the heated upper and insulated lower wall-mounted $45°$ V-upstream shaped baffles can effectively enhance the heat transfer phenomenon in a rectangular channel.

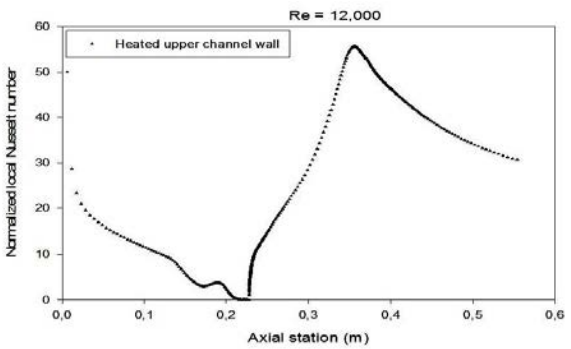

Fig. 10: Normalized local Nusselt number distribu- tion along the heated upper channel wall length at $Re = 12,000$.

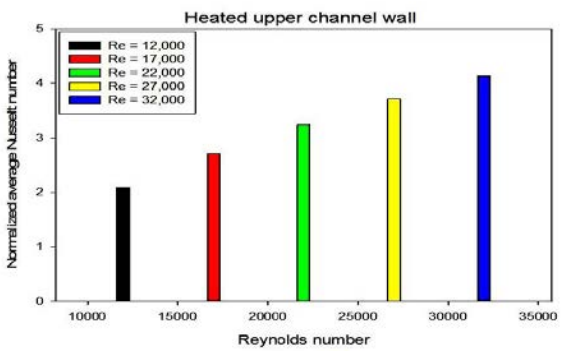

Fig. 11: Normalized average Nusselt number ver- sus Reynolds number.

The heat transfer is calculated and shown in this CFD analysis in terms of the normalized local Nusselt number which can be defined by Eq. (27). The computational result of the local heat transfer rate evolution at the heated top surface in the channel with $45°$ V-upstream baffles when $Re = 12,000$ is shown in Fig. 10. In this configuration, the insertion of the top wall V-baffle at the beginning of the heated section ($L_1 = 0.218m$) disturbs the boundary layer formation and contributes to higher heat transfer[22]. As expected, the local Nusselt number is quite high at the start of the computational domain due to the development of the thermal boundary layer[22]. The figure shows that in the region upstream of the first heated upper wall-mounted 45V-upstream baffle, the heat transfer rate shows a decrease and then goes up and down when approaching this same considered baffle. The figure also shows that the minimum heat transfer rate is located approximately at the same horizontal location that corresponds to the inserted position of the heated upper surface-attached V-upstream baffle. In the regions downstream of the V-baffle at locations corresponding to the recirculation zones

as shown in the figure, the local heat transfer rate increase gradually. This improvement is due to the intense mixing by the vortex[17]. It also indicates that the upper local heat transfer rate can be observed at the regions of high velocity especially at the top front of the insulated bottom surface-mounted $45°$ V-upstream shaped baffle, due to the strong deformation in the flow direction in those regions. However, the local heat transfer rates show a rapid reduction to a minimum value when approaching the channel exit, where the effect of the vortex mixing is diminishing[17]. The variation of the normalized average Nusselt number with Reynolds number along the heated upper channel wall is shown in Fig. 11. In the figure, there is a linear increment between average heat transfer rate and flow rate.

4.3 Skin friction coefficients

Skin friction coefficient is calculated from its definition as given in Eq. (25). As shown in Fig. 12, the largest variations in the skin friction coefficient are found at the upper front of the insulated lower wall-placed $45°$ V-upstream baffle, due to the strong velocity gradients in that region. At the start of the computational domain, the skin friction coefficients tend to drop significantly to almost zero when it reaches and passes the heated upper surface-attached $45°$ V-upstream shaped baffle. Behind this same baffle, the skin friction coefficients show an rise at the stations corresponding to the recirculation cells and drop for reaching the second V-baffle and then rise near the upper corner of this same obstacle to a peak before decreasing rapidly through the exit, meaning that the pressure in that location is below atmospheric pressure[13]

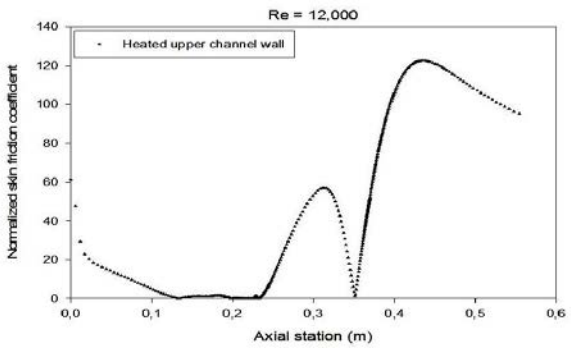

Fig. 12: Normalized skin friction coefficient distribution along the heated upper channel wall length at Reynolds number $Re = 12,000$.

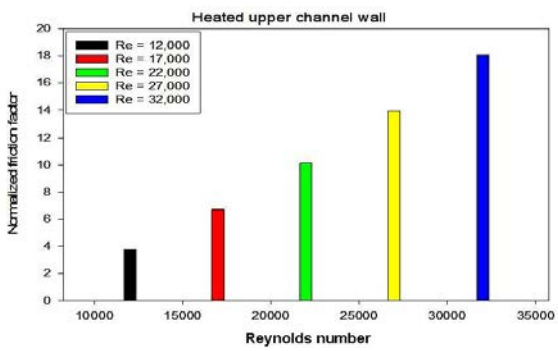

Fig. 13: Normalized friction factor versus

The skin friction loss is also affected by the flow Reynolds value. The friction factor was computer from the pressure across the computational flow domain, using Darcy Weisbach formula as given in Eq. (26). Fig. 13 shows the friction factor versus the Reynolds number in the case of the investigated configuration. The friction factor is normalized by the Petukhov correlation[23] (see Eq. (31)).

$$f_0 = (0.79 \ln \mathrm{Re} - 1.64)^{-2} \quad \text{for} \quad 3 \times 10^3 \leq \mathrm{Re} \leq 5 \times 10^6 \tag{31}$$

In the figure, a rise in the normalized friction factor is noted with an augmentation in the flow rate. This can be attributed to the fact that augmenting the flow rate can induce higher recirculation flows before and after the heated upper and insulated lower wall-mounted $45°$ V-upstream baffles leading to higher recirculation lengths and heights, improving the convective heat transfer rate and skin friction loss especially for higher flow rate.

4.4 Performance evaluation

Fig. 14 shows the evolution of the thermal enhancement factor (TEF), calculated by Eq. (32), as a function of Reynolds number ($Re = 12,000, 17,000, 22,000, 27,000$, and $32,000$) with a constant section of the V-baffles for the lower surface of the hot wall of the channel.

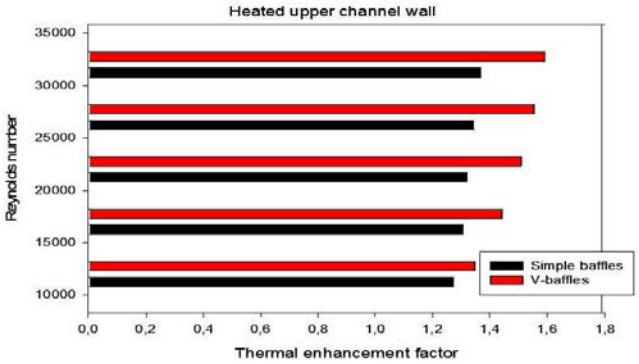

Fig. 14: Performance evaluation for both simple and V-baffles

The following expression represents the thermal enhancement factor (TEF):

$$TEF = (Nu/Nu_0) \Big/ (f/f_0)^{1/3} \tag{32}$$

5 Conclusion

Through this simulation, an analysis was conducted to examine the thermal and aerodynamic fields of air inside a 2D horizontal rectangular section channel. Two transverse, staggered, 45° V-upstream shaped, solid-type baffles were inserted into the channel in order to develop vortices to improve the mixing, and consequently the heat transfer. The steady-state turbulent flow equations were solved using the finite volume method. In particular, contour plots of streamlines, fields of velocity and temperature, profiles of axial velocity, normalized local and average coefficients of skin friction, normalized local and average numbers of Nusselt, and factor of thermal enhancement were obtained and investigated numerically. The present numerical results in terms of axial velocity profiles were compared with the experimental ones found in the literature. This comparison indicates that a qualitative agreement and a very good concordance exist between the two results. The results obtained in the present smooth rectangular channel agree pretty well within the range 3.5% for the Nusselt number Dittus-Boelter correlation. Important deformations and large recirculation regions were observed in the flow field. Typically, the intensity of the vortices depends heavily on the functioning parameters of the model under consideration. It is widely admitted that their lengths are directly proportional to the Reynolds number. The present flow structure has significant influences on the temperature field distributions in the entire domain under investigation. The hottest regions are generally located in the neighborhood of the heated top surface and the tips of the V-fin. The largest value of the axial variations of the Nusselt number and skin friction coefficient is found in the region facing the V-baffle, while the smallest value is in the region near the V-fin. The channel containing the V-obstacles with a large Reynolds number gave higher heat transfer, friction loss, and thermal enhancement factor than the one with a smaller Reynolds number. This simulation can be applied in improving the thermal efficiency of heat exchangers as well as solar air baffled channel collectors.

References

[1] M. A.Saini, V.K.K. Two dimensional model of pulsatile flow of a dusty fluid through a tube with axisymmetric constriction. *World Journal of Modelling and Simulation*, 2016, **12**(1): 70–78.

[2] P. A.Saini, VK.Katiyar. Numerical simulation of gas flow through a biofilter in lung tissues. *World Journal of Modelling & Simulation*, 2015, **11**(1): 33–42.

[3] M. A.Valencia. Turbulent unsteady flow and heat transfer in channels with periodically mounted square bars. *International Journal of Heat & Mass Transfer*, 2002, **45**(8): 1661–1673.

[4] D. B.E.Launder. The numerical computation of turbulent flows. *Computer Methods in Applied Mechanics & Engineering*, 1974, **3**(2): 269–289.

[5] S., B.K.P.A., M.S.L. The effect of the inclined perforated baffle on heat transfer and flow patterns in the channel. *International Communications in Heat & Mass Transfer*, 2012, **39**(10): 1578–1583.
[6] S. M. B.P.Leonard. Ultra-sharp nonoscillatory convection schemes for high-speed steady multidimensional flow. 1990.
[7] D. C.Berner, F.Durst. Flow around baffles. *Journal of Heat Transfer*, 1984, **106**(4): 743–749.
[8] P., E.A.H, D.I. Numerical studies on the effect of delta-shaped obstacles spacing on the heat transfer and pressure drop in v-corrugated channel of solar air heater. *Solar Energy*, 2016, **131**: 47–60.
[9] L. F.W.Dittus. Heat transfer in automobile radiator of the tubular type. *International Communications in Heat & Mass Transfer*, 1985, **12**(1): 3–22.
[10] L. JR.Lopez, NK.Anand. Heat transfer in a three-dimensional channel with baffles. *Numerical Heat Transfer*, 1996, **30**(2): 189–205.
[11] K. K. Elangovan. Mhd peristaltic flow of blood through porous medium with slip effect in the presence of body acceleration. *World Journal of Modelling and Simulation*, 2017, **13**(2): 151–160.
[12] K. M. Kelkar. *Numerical prediction of fluid flow and heat transfer in a parallel plate channel with staggered fins /*. Hemisphere Pub. Corp. ;, 1987.
[13] S. LC.Demartini, HA.V. Numeric and experimental analysis of the turbulent flow through a channel with baffle plates. *Journal of the Brazilian Society of Mechanical Sciences & Engineering*, 2004, **26**(2): 153–159.
[14] M., MA.H., AM.M. Experimental investigation of heat transfer and flow over baffles of different heights. *Journal of Heat Transfer*, 1994, **116**(2): 363–368.
[15] K., M.M.Pirouz, M.F. Lattice boltzmann simulation of conjugate heat transfer in a rectangular channel with wall-mounted obstacles. *Scientia Iranica*, 2011, **18**(2): 213–221.
[16] S. N.Ahmed, U.Khan. Two-dimensional flow of a jeffery fluid in a dilating and squeezing porous channel. *World Journal of Modelling & Simulation*, 2016, **12**(1): 59–69.
[17] M. Nasiruddin, Siddiqui. Heat transfer augmentation in a heat exchanger tube using a baffle. *International Journal of Heat & Fluid Flow*, 2007, **28**(2): 318–328.
[18] H. N.Guerroudj. Mixed convection in a channel provided with heated porous blocks of various shapes. *Energy Conversion & Management*, 2010, **51**(3): 505–517.
[19] H. O.R.Motlagh. Novel approach to modelling of turbulent flows. *World Journal of Modelling and Simulation*, 2010, **6**(4): 243–256.
[20] S. D. P Dutta. Effect of baffle size, perforation, and orientation on internal heat transfer enhancement. *International Journal of Heat & Mass Transfer*, 1998, **41**(19): 3005–3013.
[21] S. V. Patankar. *Numerical heat transfer and fluid flow*. Hemisphere Pub. Corp., 1980.
[22] A. P.Dutta. Internal cooling augmentation in rectangular channel using two inclined baffles. *International Journal of Heat & Fluid Flow*, 2005, **26**(2): 223–232.
[23] B. S. Petukhov. Heat transfer and friction in turbulent pipe flow with variable physical properties. *Advances in Heat Transfer*, 1970, **6**: 503–564.
[24] B. R.Karwa. Heat transfer and friction in an asymmetrically heated rectangular duct with half and fully perforated baffles at different pitches. *International Communications in Heat & Mass Transfer*, 2009, **36**(3): 264–268.
[25] H., R.Saim, H.B. A computational work on turbulent flow and heat transfer in a channel fitted with inclined baffles. *Heat & Mass Transfer*, 2013, **49**(6): 761–774.
[26] H., R.Saim, H.B. Turbulent flow and heat transfer enhancement of forced convection over heated baffles in a channel. *International Journal of Numerical Methods for Heat & Fluid Flow*, 2013, **volume 23**(4): 613–633(21).
[27] K. S.Kumar, KV.Karanth. Numerical study of heat transfer in a finned double pipe heat exchanger. *World Journal of Modelling & Simulation*, 2015, **11**(1): 43–54.
[28] P. S.Sripattanapipat. Numerical analysis of laminar heat transfer in a channel with diamond-shaped baffles. *International Communications in Heat & Mass Transfer*, 2009, **36**(1): 32–38.
[29] P. S.Sriromreum, C.T. Experimental and numerical study on heat transfer enhancement in a channel with z-shaped baffles . *International Communications in Heat & Mass Transfer*, 2012, **39**(7): 945–952.
[30] G. SV.Moller, LAM.Endres. Wall pressure field in a tube bank after a baffle plate. **in:** *Transactions of SMiRT 15 - 15th International Conference on Structural Mechanics in Reactor Technology 7*, 1999, 262–275.
[31] E. S. SV.Patankar, CH.Liu. Fully developed flow and heat transfer in ducts having streamwise-periodic variations of cross-sectional area. *Journal of Heat Transfer*, 1977, **99**(2): 180.
[32] S. T.Das. A 2-d numerical study on flow characteristics for four different types annular dump combustor models. *World Journal of Modelling and Simulation*, 2015, **11**(3): 208–218.
[33] P. P. W.J., N.J. 3d numerical study on flow structure and heat transfer in a circular tube with v-baffles . *Chinese J. Chemical Eng*, 2015, **23**(2): 342–349.
[34] A. W.Jedsadaratanachai. Effects of blockage ratio and pitch ratio on thermal performance in a square channel with 30 double v-baffles. *Case Studies in Thermal Engineering*, 2014, **4**(C): 118–128.

[35] J. Y.L.T., T.S.Chang. Heat transfer enhancement of backward-facing step flow in a channel by using baffle installation on the channel wall. *Acta Mechanica*, 2005, **174**(1-2): 63–76.

[36] Y.Menni,A.A., C.Z. Numerical analysis of turbulent forced-convection flow in a channel with staggered l-shaped baffles. *J. New Technology and Materials*, 2016, **6**(2): 44–55.

[37] Y.Menni,A.A., C.Z. Constant property newtonian fluid flow and heat transfer over cascaded fins. *Revue des Energies Renouvelables*, 2017, **20**(1): 25–38.

[38] Y.Menni,A.A., C.Z. Numerical analysis of turbulent forced convection in a channel with flat and diamond-shaped baffles of different heights. *Courrier du Savoir*, 2017, **23**: 75–84.

[39] Y.Menni,A.A., C.Z. Numerical study of heat transfer and fluid flow in a channel with staggered arc-shaped baffles. *Communication Science & Technology*, 2017, **18**: 43–57.

[40] Y.Menni,A.A., C.Z. Use of waisted triangular-shaped baffles to enhance heat transfer in a constant temperature-surfaced rectangular channel. *J. Eng. Science and Technology*, 2017, **12**(12): 3251–3273.

[41] Y.Menni,A.A., C.Z. Numerical analysis of thermal and aerodynamic fields in a channel with cascaded baffles. *Periodica Polytechnica Mechanical Engineering*, 2018, **62**(1): 16–25.

[42] Y.Menni,A.A., C.Z. Etude numerique comparative entre deux types de chicanes et ailettes (rectangulaire et rectangulaire arrondie) utilisees pour ameliorer les performances des capteurs solaires plans a air. *Revue des Energies Renouvelables*, 2015, **18**(3): 347–361.

[43] Y.Menni,A.A., C.Z. Computational analysis of heat transfer and fluid flow characteristics over flat bars of different height. *Revue des Energies Renouvelables*, 2016, **19**(3): 345–366.

[44] Y.Menni,A.A., C.Z. Computational analysis of turbulent forced convection in a channel with staggered corrugated baffles. *Communication Science & Technology*, 2016, **16**: 34–43.

[45] Y.Menni,A.A., C.Z. Numerical study of turbulent heat transfer in a trapezoidal channel with flat baffles. *Communication Science & Technology*, 2016, **17**(3): 67–77.

[46] N. A. Z. Guo. Three-dimensional heat transfer in a channel with a baffle in the entrance region. *Numerical Heat Transfer*, 1997, **31**(1): 21–35.